CONF-960643--3

Martin L. Grossbeck[1], Loy T. Gibson[2], Shiro Jitsukawa[3], Louis K. Mansur[4], and Lloyd J. Turner[5]

IRRADIATION CREEP AT TEMPERATURES OF 400°C AND BELOW FOR APPLICATION TO NEAR-TERM FUSION DEVICES

REFERENCE: Grossbeck, Martin L., Gibson, Loy T., Jitsukawa, Shiro, Mansur, Louis K., and Turner, Lloyd J., "Irradiation Creep at Temperatures of 400°C and Below for Application to Near-Term Fusion Devices", Effects of Radiation on Materials: 18th International Symposium, ASTM STP 1325, Randy K. Nanstad, Ed., American Society for Testing and Materials, 1997.

ABSTRACT: To study irradiation creep at 400°C and below, a series of six austenitic stainless steels and two ferritic alloys was irradiated sequentially in two research reactors where the neutron spectrum was tailored to produce a He production rate typical of a fusion device. Irradiation began in the Oak Ridge Research Reactor; and, after an atomic displacement level of 7.4 dpa, the specimens were moved to the High Flux Isotope Reactor for the remainder of the 19 dpa accumulated. Irradiation temperatures of 60, 200, 330, and 400°C were studied with internally pressurized tubes of type 316 stainless steel, PCA, HT 9, and a series of four laboratory heats of: Fe-13.5Cr-15Ni, Fe-13.5Cr-35Ni, Fe-13.5Cr-15Ni-0.18Ti, and Fe-16Cr. At 330°C, irradiation creep was shown to be linear in fluence and stress. There was little or no effect of cold-work on creep under these conditions at all temperatures investigated. The HT9 demonstrated a large deviation from linearity at high stress levels, and a minimum in irradiation creep with increasing stress was observed in the Fe-Cr-Ni ternary alloys.

KEYWORDS: irradiation creep, ferritic, austenitic, stress, helium, deformation

---

[1]Senior Research Staff Member, Oak Ridge National Laboratory, Oak Ridge, TN, 37831-6376

[2]Technologist, Oak Ridge National Laboratory, Oak Ridge, TN, 37831-6376

[3]Research Scientist, Tokai Research Establishment, Japan Atomic Energy Research Institute, Ibaraki-ken, Japan 319-11

[4]Group Leader, Oak Ridge National Laboratory, Oak Ridge, TN, 37831-6376

[5]Supervisor, Oak Ridge National Laboratory, Oak Ridge, TN, 37831-6030

INTRODUCTION

In addition to radiation, the first wall and blanket structures of a fusion device will experience stresses from thermal loading, from swelling, and from primary loads on the structure itself. Irradiation creep, which requires the simultaneous presence of both radiation and stress, will cause measurable deformation at temperatures far below those that would produce significant thermal creep. The effects of irradiation can be both harmful and beneficial. Relief of swelling stresses and constant thermal stresses are examples of beneficial effects. Deformation in response to primary loads is a harmful effect that must be accounted for in the design of any fusion device.

Near-term fusion test devices will operate at lower temperatures than power production devices. Irradiation creep, which has historically been investigated at temperatures above 400°C, is still operative even at cryogenic temperatures [1]. Unlike thermal creep, it is not only operative, but in some cases larger creep deformations are produced at lower temperatures. The present study addresses temperatures below 400°C, applicable to such fusion devices as the ITER, International Thermonuclear Experimental Reactor.

Irradiation creep was first observed over 40 years ago in uranium [2]. Since that time the phenomenon has been studied extensively around the world, mostly in connection with liquid metal breeder reactor programs. Because of the application to liquid metal cooled reactors, nearly all of the investigations were made at temperatures above 400°C. Limited research was done at lower temperatures mostly at low fluence levels. Experiments conducted by Hesketh, in the Herald reactor, demonstrated higher levels of irradiation creep in Ni and Zircaloy-2 at -195°C than at elevated temperatures [1]. As part of the present study, higher levels of irradiation creep were observed in the Oak Ridge Research Reactor (ORR) at 60°C than at either 200, 330, or 400°C. This result was interpreted in terms of the larger concentration of interstitial point defects that persist for extended periods at the lower temperatures. These excess interstitials give rise to dislocation climb followed by glide and thus plastic deformation [3],[4]. This explanation is consistent with the observations of Hesketh.

EXPERIMENTAL METHODS

Stresses as high as 490 MPa, depending upon the alloy, were applied using internally pressurized tube specimens 4.57 mm in diameter and 25.4 mm long. The tube wall thickness was 0.25 mm for all specimens except those of HT9 for which it was 0.18 mm. The tubes were profiled with a non-contacting laser micrometer system with a precision of ±250 nm. A series of 500 measurements was taken in a helical pattern along each tube, but only the central 300 measurements were used in the computations of creep rates in order to avoid any mechanical restraints that might be imposed by the welded end caps. However, the complete set of measurements was used as an aid in evaluation of the tube profile and in determining validity of the measurements. The tubes were measured

prior to pressurization and after pressurization with helium; the degree of elastic deformation was used to determine leaking tubes. The tubes were again measured with the same instrument following irradiation. Zero pressure tubes, more correctly called rings since they were shorter than the pressurized tubes and had no end caps, were included in the irradiation to permit correction for irradiation-induced swelling. Swelling corrections were applied to only the 400°C data since only these specimens showed measurable swelling.

The alloys investigated consisted of two fusion candidate austenitic stainless steels: AISI type 316 stainless steel melted in Japan (J316) in both annealed and 20% cold-worked conditions [5], and two heats of the Fusion Program primary candidate alloy, PCA, one a U.S. heat [6], designated USPCA in the 25% cold-worked state and the

Table 1 Chemical Composition of Alloys (wt.%)

Element	USPCA	JPCA	J316	Fe-13.5Cr-15Ni	Fe-13.5Cr-35Ni	Fe-13.5Cr-15Ni-0.18Ti	HT9	Fe-16Cr
B	0.00003	0.003						
C	0.05	0.06	0.06					
Co	0.003	0.002	<0.1					
Cr	14.0	14.2	16.8	13.0	13.5	13.9	12.0	16.5
Cu				0.002	0.002		0.001	
Fe	bal	bal	bal					
Mn	1.8	1.8	1.8				0.61	
Mo	2.3	2.3	2.5				0.99	
Ni	16.3	15.6	13.5	13.6	30.5	14.5	0.93	
P	0.01	0.027	0.028			<0.05		
Si	0.44	0.50	0.61	0.13	<0.05	0.18	0.16	<0.05
Ti	0.24	0.24	0.05					
V							0.40	
W							0.80	

other a Japanese heat, designated JPCA, in the solution annealed condition [7]. Three austenitic Fe-Ni-Cr laboratory melted alloys were used to compare the rates of irradiation creep with the rates of swelling: Fe-13.5Cr-15Ni, Fe-13.5Cr-35Ni, and Fe-13.5Cr-15Ni-0.18Ti (previously reported as 0.25 Ti), all in the solution annealed condition [8]. The alloys Sandvik HT9 and a laboratory heat of the pure binary Fe-16Cr represented the ferritic/martensitic group of alloys. The chemical compositions of all the alloys appear in Table 1. The USPCA and the HT9 specimens were prepared from seamless drawn tubing, and the specimens of the other alloys were machined from rod. End caps were electron-beam-welded into place, one cap with a hole to allow pressurization. The tubes were internally stressed by pressure charging with helium and sealed using laser welding

in a pressure chamber with sapphire windows. Maximum stresses were selected to be typically about two-thirds of the yield stress with the highest being 490 MPa. High stresses were selected in order to insure measurable deformations even at the risk of tube rupture.

Irradiation was begun in the ORR with the specimens at four temperatures. Those at 60°C were in contact with reactor coolant water. Those at 200°C were in helium, and those at 330 and 400°C were in a NaK environment. Temperature control in the ORR was achieved by surrounding the specimen chambers by an annulus filled with a mixture of helium and neon or helium and argon. By adjusting the gas composition, thermal conductivity could be adjusted to achieve the desired temperature as determined by 17 thermocouples located in the capsules. Dosimetry indicated that 6.9 dpa had been achieved in the 60 and 200°C specimens and 7.4 dpa in the 330 and 400°C specimens. The irradiation parameters are summarized in Table 2. The diameters of the pressurized tubes were then measured and results reported [3],[4]. The specimens were then re-encapsulated and irradiated in the High Flux Isotope Reactor (HFIR).

In the HFIR, specimens were irradiated as closely as possible to the temperature of irradiation in the ORR. The 60°C specimens were again irradiated in contact with reactor coolant water, and the others were irradiated in a helium environment.

The HFIR is a mixed spectrum research reactor using 93% enriched uranium oxide fuel and moderated with ordinary water. It has a central flux trap for high flux irradiations and isotope production. The core is surrounded by a beryllium reflector. The present irradiation was conducted in the inner portion of the reflector in a position known as the RB* position. The capsule was surrounded by a 4.2 mm hafnium shield in order to reduce the thermal neutron flux in order to achieve the desired helium to dpa ratio. The total flux level in this shielded position was measured to be 8.7×10^{18} n/m^2-s, with thermal flux 1.05×10^{18} n/m^2-s, and fast flux $4.3\ 10^{18}$ n/m^2-s (E>0.1 MeV). Since the 60°C specimens were in direct contact with reactor coolant, their temperature was assured without recourse to thermocouples. Temperatures for the elevated temperature capsules were controlled using gas mixtures similar to those used in the ORR. The average reading of a series of 21 thermocouples was used to control temperature. The design temperatures were held to within ±25°C throughout the capsules during the duration of the irradiation. Dosimetry indicated that an additional 11.6 dpa was achieved in the 60 and 330°C specimens, and reactor power measurements were used to calculate an additional displacement level of 9.9 dpa in the 200 and 400°C capsules. The total displacement levels achieved from both irradiations were 18.5 dpa for the 60°C specimens, 16.8 dpa for the 200°C specimens, 19.0 dpa for the 330°C specimens, and 17.3 dpa for the 400°C specimens as shown in Table 2. For simplicity, the final displacement levels were rounded to 19 dpa in this paper. Helium levels are also presented in Table 2; they were obtained from inert gas fusion mass analysis [9]. The helium/dpa levels are also presented in Table 2. These values were determined for type 316 stainless steel, assuming 13% nickel. The values are higher for PCA, as can be determined by multiplying by the ratio of nickel concentrations in the two alloys.

However, values of He/dpa for all of the austenitic alloys are within the range expected for a fusion reactor with a lithium blanket.

Table 2 Irradiation Parameters

	ORR			HFIR			Total Combined		
Temperature (°C)	dpa	He†	He/dpa†	dpa	He†	He/dpa†	dpa	He†	He/dpa†
60	6.9	75	11	11.6	110	9.5	18.5	190	10
200	6.9	75	11	9.9*	90*	9.1*	16.8*	170*	10*
330	7.4	100	14	11.6	120	10	19.0	225	12
400	7.4	100	14	9.9*	100*	10*	17.3*	200*	12*

* Calculated from reactor power and previous dosemetry

† For type 316 stainless steel

For the 60° tubes, the move from the ORR to the HFIR complicated the analysis of their creep responses. The higher pressure of the HFIR coolant water on these tubes reduced the stresses in the walls of the tubes. The external pressure on the 60° tubes was 210 kPa gage in the ORR but 2.57 MPa gage in the HFIR. Because the pressurized tubes were designed for irradiation in the ORR, the stresses in the tubes were considerably lower when the tubes were transferred to the HFIR. The laboratory heats of the pure austenitic and the Fe-16Cr alloys were affected most, since these alloys were weak and had to be stressed to low levels originally. In this case a few tubes were actually in compression in the HFIR. However at 60°C, about 20% of the tubes failed, probably during the ORR irradiation or by corrosion in the interim between irradiations while they were stored in a radiation hot cell. Because of these difficulties with the 60°C specimens, their higher dpa results are not reported.

RESULTS AND DISCUSSION

Specimen Profiles

A representative set of tube profiles is shown in Fig. 1. The specimens were all fabricated from the same length of PCA tubing and pressurized to attain the mid-wall hoop stresses given in the figure. The sinusoidal patterns arise from two sources. The first source of the oscillations is that the tubes are not round to within the precision of the measurement. The second source arises from the inability to align the tubes with

the axis of rotation on each end. Since the tubes are displaced different amounts at the two ends, they will precess. A combination of precession and elliptical shape can result in a compound cyclic pattern such as results from the superposition of two sinusoidal wave forms with a phase difference. A pattern of this type exists for one of the 172 MPa specimens in Fig. 1. Dust particles on the specimen are shown by the isolated high narrow peaks seen in the 346 MPa curve. This particular curve yields a good measurement since only the center three fifths of the curve is used. Notice that increasing levels of applied stress cause clear and progressive separation of the diameter (strain) profiles and that the amplitude of the oscillations is small compared to the plastic deformation of the tubes. Despite the differences in oscillations in the two 172 MPa curves, they almost superimpose, indicating a high level of reproducibility.

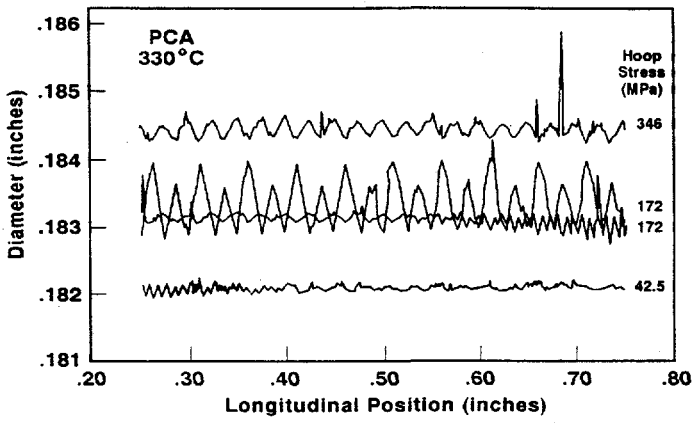

Figure 1 Laser Profilometer traces from four representative tubes of USPCA.

Temperature Dependence

In the previously reported work on the 60°C specimens irradiated in the ORR, large rates of irradiation creep were observed [3]. Since irradiation creep arrises from the behavior of point defects produced during irradiation, the low temperature irradiation creep can be understood by examination of the equations for point defect concentrations. Solving the point defect rate equations, (1) and (2), without the assumption of steady state, predicts the accelerated low temperature irradiation creep. The phenomenon arises because a transient period (which could be longer than the total period of irradiation) occurs, during which the interstitial concentration is elevated but where vacancies are not sufficiently mobile, due to the low temperature, to cancel the effects of the interstials on dislocation climb.

$$\frac{dC_v}{dt} = G_v - RC_vC_i - K_vC_v \quad (1)$$

$$\frac{dC_i}{dt} = G_i - RC_vC_i - K_iC_i \quad (2)$$

$C_{v,i}$ = vacancy, interstitial concentration
$G_{v,i}$ = vacancy, interstitial generation rate
R = point defect recombination coefficient
$K_{v,i}$ = rate constants for loss of vacancies and interstitials to sinks.

In addition to the high level of irradiation creep at 60°C, the rate equations predict a low rate of creep in the region of 200°C for austenitic stainless steels as shown in Fig. 2 [10]. The data points shown on the curves are from the ORR portion of the present experiment. The agreement is perhaps somewhat fortuitous, considering the assumptions that were necessary for the calculations. Nonetheless, it demonstrates accelerated irradiation creep at low temperatures and a minimum in irradiation creep as temperature increases. The minimum, at about 200°C for stainless steel, is attributed to the increase in vacancy diffusion with increasing temperature which causes enhanced recombination of vacancies and interstitials at dislocations and shortens the transient period of increased interstitial concentration. As temperature increases still further above 200°C, increased diffusivities cause the irradiation creep rate to increase as the steady state processes of climb by the Stress Induced Preferred Absorption (SIPA) and Preferred Absorption Glide (PAG) control behavior.

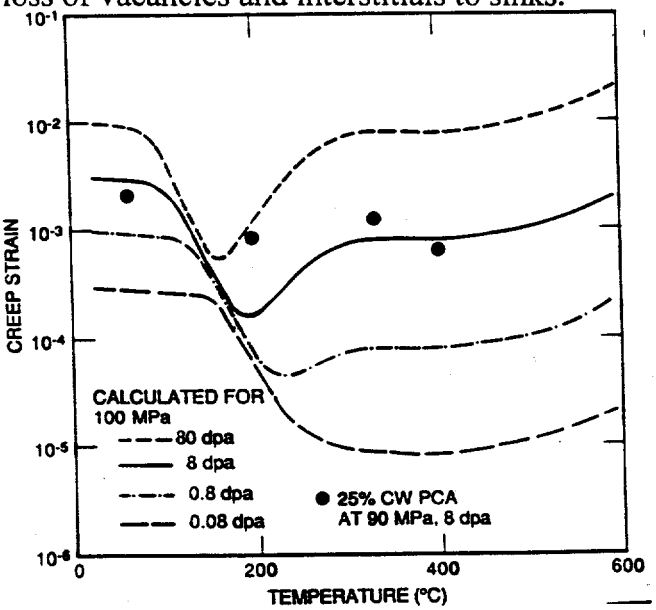

Figure 2 Calculated curves of irradiation creep in austenitic stainless steel as a function of temperature and displacement damage. The data points are results from the present specimens for the 7-8 dpa irradiation.

Austenitic Stainless Steels

Results for type 316 stainless steel are shown in Fig. 3, where effective uniaxial strain is plotted as a function of effective uniaxial mid-wall stress [11]. Each point on the curve represents one tube specimen, and the 7 dpa results are shown for comparison with the recent 19 dpa results. The creep coefficients are also shown in Table 3 where the lower creep rates at 200°C are most evident at 19 dpa. The deformations at 7 dpa were too small to provide accurate irradiation creep rates. The similarity between solution annealed and cold-worked alloys is also evident at all

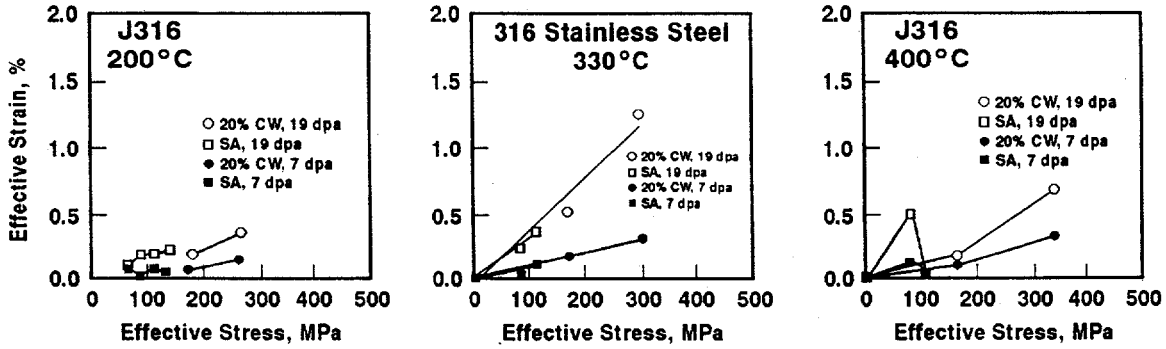

Figure 3 Irradiation creep strain in type 316 stainless steel in terms of effective uniaxial stress and strain for 7 and 19 dpa.

Table 3 Irradiation Creep Coefficients (% MPa^{-1} dpa^{-1} x 10^{-4})

	0-7 dpa				0-19 dpa		
	60°C	200°C	330°C	400°C	200°C	330°C	400°C
USPCA 25% CW	9.2-14	.93	2.3 ± .1	1.8	0.63 ± .03	2.7 ± .08	1.5 ± .1
JPCA SA	5.1	1.9	1.6 ± .7	3.5	0.90 ± 0.3	2.7	4.1
J316 20% CW	2.2	1.1	1.3 ± .1	1.3	0.70 ± .09	2.1 ± .4	1.1 ± .2
J316 SA	2.2	1.1	1.4 ± .7	1.4	0.75 ± .3	1.7 ± .2	3.2
Fe-13.5E-15Ni					2.7 ± .3	0.8 ± 2	
Fe-13.5E-35Ni					2.4 ± .2	3.4 ± .4	
Fe-13.5Cr-15Ni-.18Ti					1.6 ± .03	5.5 ± .6	
HT-9		0.38	0.38	0.61	0.38 ± .1	0.43 ± 0.8	1.1 ± .2/11
Fe-16Cr		1.7	0.82	1.6	0.50	0.5 ± .2	1.5 ± .7

three temperatures. The drop in deformation as stress increases at 400°C is clearly the result of at least one leaking or failed tube. The linearity in stress and fluence is evident at all temperatures.

The standard errors are given in Table 3; however, these reflect only the statistics of the curve fitting routine. It is not uncommon to observe a factor of two variation in irradiation creep rates between two reactors. Temperature variation between specimens irradiated in the same capsule can also account for large variations in irradiation creep rates since temperature determines gas pressure and thus stress. Nonetheless, the standard errors in the table indicate cases where there were few data points and large scatter.

A similar set of curves is shown in Fig. 4 for PCA. As with type 316 stainless steel, there is a low rate of irradiation creep at 200°C. There were more specimens and thus more stress levels for this alloy in the cold-worked state than any of the other alloys. The additional specimens provide clear evidence for the linearity in stress and fluence, over the range of parameters investigated. The absence of an effect of cold-work level is also evident, although it could not be demonstrated at 400°C because of leakage or failure of annealed tubes.

As will be seen later in equation (3), the expression for irradiation creep by the SIPA mechanism, there is a linear dependence of creep rate on dislocation density.

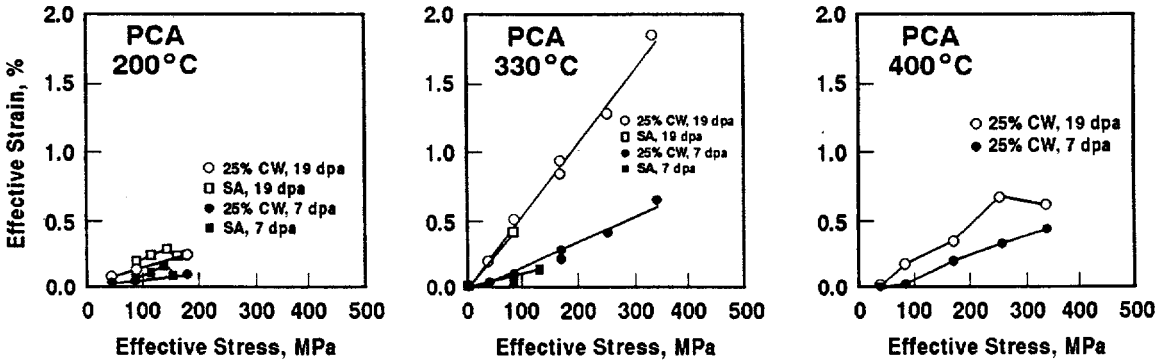

Figure 4 Irradiation creep strain in PCA in terms of effective uniaxial stress and strain for 7 and 19 dpa.

This would at first lead one to expect an effect of cold-work level on irradiation creep rate. However, in the sink-dominated regime, the inverse dependence of the interstitial concentration on dislocation density cancels the direct dependence of the creep rate and results in irradiation creep that is independent of the dislocation density [12],[13].

A set of three laboratory heats of austenitic alloys was selected for comparison of irradiation creep in cases of different swelling. The pure ternary alloy Fe-13.5Cr-

15Ni was selected because of its rather high swelling rate and Fe-13.5Cr-35Ni was selected because of its low swelling rate as determined by Bates and Johnston [14]. The alloy considered high swelling was also made swelling resistant by the addition of 0.18% titanium [8].

The curves for the 200°C case are shown in Fig. 5. For this figure, the scale has been changed to show detailed behavior since the slopes of the curves are significantly lower than those at higher temperatures, as predicted from the theory and as observed in the other austenitic stainless steels. The expected linear relationships with stress and fluence are valid, and at this temperature, the issue of swelling does not enter, so these results will not be discussed in detail.

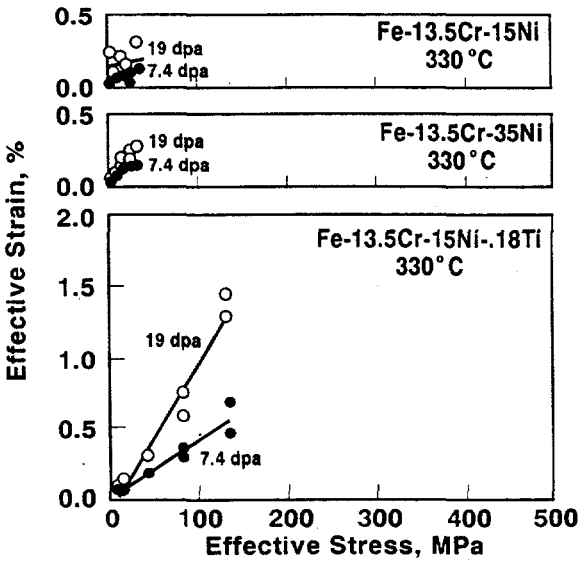

Figure 5 Irradiation creep strain for three laboratory heats of stainless steels at displacement levels of 7.4 and 19 dpa at 330°C. The scales were chosen for comparison with other austenitic alloys.

Curves for irradiation creep in these alloys at 330°C appear in Fig. 6. The axes of the graphs have been kept the same as for the earlier figures in order to preserve the scale for comparison of one alloy with another. In the case of Fe-13.5Cr-15Ni, the data are too scattered at 19 dpa to extract any meaningful information. The curves for the Fe-13.5Cr-35Ni alloy are well behaved even though only low stresses were investigated because of the low strength of the alloy. In the case of the titanium doped alloy, the previously observed linear relationships are easily observed. The creep rate is significantly higher for this alloy than for the pure ternaries as seen in Table 3. The reason for the higher irradiation creep rate in this alloy remains under investigation. However, it is consistent with the behavior of the alloy PCA which is also a titanium-doped alloy. It is possible to speculate about a mechanism involving titanium-rich precipitates in both cases. The TiO phase, which is less dense than the alloy matrix, has been observed to be the dominant precipitate in the Fe-13.5Cr-15Ni-0.18Ti alloy [8]. Accommodation of the volume expansion associated with the formation of TiO causes preferential absorption of vacancies, just as suggested in the case of PCA, with TiC [15]. It is suggested that the resulting defect imbalance toward a higher interstitial flux to dislocations could lead to a slightly higher rate of irradiation creep.

The most interesting results appear in Fig. 7 where the 400°C data are plotted for this set of alloys. At 19 dpa all three of the alloys exhibit a minimum with increasing stress. At 7 dpa the trends are also visible but not yet clearly defined. This is clearly an unexpected result and difficult to understand. In order to establish that there actually was gas in the tubes and that the stress did in fact increase monotonically as shown, the tubes were punctured following irradiation. The pressure of the released gas was measured and the pressures and thus stress levels were confirmed. Since the trends are well within the capability of the measurement instruments, it is

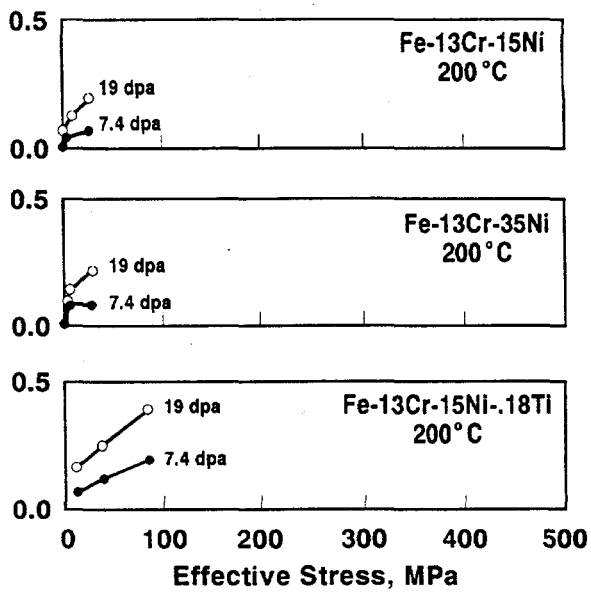

Figure 6 Irradiation creep strain for three laboratory-melted austenitic alloys at displacement levels of 7.4 and 19 dpa at 200°C.

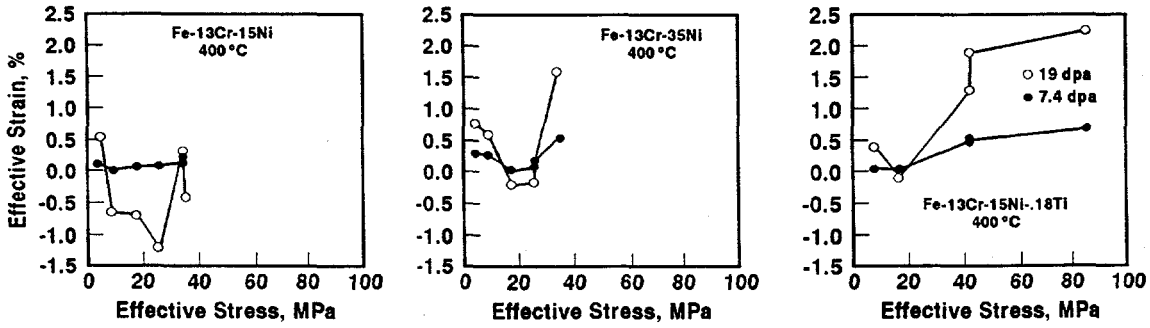

Figure 7 Irradiation creep strain for three laboratory heats of stainless steels at displacement levels of 7.4 and 19 dpa and a temperature of 400°C.

apparent that the phenomenon is real. The most likely mechanism involves precipitation rather than irradiation creep. Densification has been observed during irradiation, mostly in cold-worked alloys; however, densification aided by increasing tensile stress is nonphysical. In the analysis of the pressurized tubes, it is assumed that the tubes are thin-walled. In the case of a thick wall, the stress at the inner surface in the radial direction is compressive and equal to the pressure of the internal gas. For a real wall, rather than an infinitely thin wall, there remains a radial compressive stress. Perhaps the nucleation of a rod-like (since there is a compressive

stress in only one direction) precipitate is aided by this stress. However, the hydrostatic stress remains tensile, further complicating this explanation. The presence of thermal gradients through the wall of the tube during irradiation also introduces compressive stresses. These stresses also might nucleate precipitates. Electron microscopy must be performed in order to establish the presence and morphology of a precipitate of lower density than the matrix in the stress regime of the minimum creep rate. At higher internal pressures, the normal tensile hoop stress in the wall prevails and irradiation creep can dominate. The suggested mechanisms are purely speculation; clearly further research must be done to elucidate the mechanism of this phenomenon.

Ferritic Steels

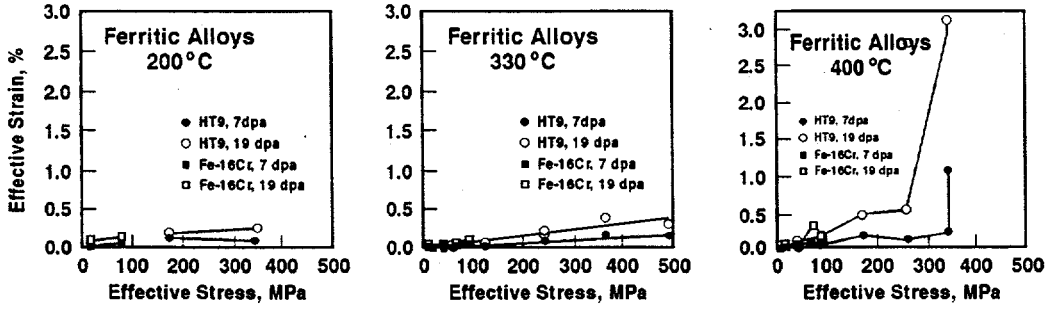

Figure 8 Irradiation creep strain as a function of stress for Sandvik HT9 and a pure binary Fe-16Cr alloy.

Irradiation creep deformations for the ferritic alloys Sandvik HT9 and the laboratory heat of Fe-16Cr appear in Fig. 8. Both alloys exhibit similar levels of irradiation creep; however, the binary alloy was too weak to obtain data at stress levels sufficiently high to give strain data without large scatter. The lower rate of irradiation creep compared with that of austenitic stainless steels is

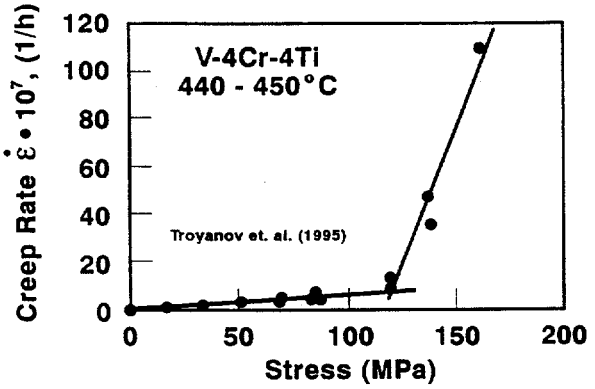

Figure 9 Irradiation creep rate as a function of stress for the alloy V-4Cr-4Ti obtained from a thin-walled tube in torsion irradiated in the BR-10 Reactor. (Reference [20])

apparent as shown in Table 3. It is also consistent with the results of previous investigators [16],[17],[18],[19]. The linear dependence on stress and fluence is difficult to discern at 200°C but is evident at 330°C. At 400°C there is what appears to be anomalous behavior at the highest stress level. Very abrupt non-linear dependence with stress is observed. The stress levels investigated in this experiment are higher than previously explored so that the results cannot be compared with the results of other investigators. It is not, however, the first time that such an abrupt increase in creep deformation has been observed in a bcc metal. Figure 9 shows irradiation creep rate as a function of stress for a vanadium alloy, V-4Cr-4Ti, as determined by helical springs [20]. In this case there are many more data so that a clear bi-linear curve is evident.

A quadratic dependence of irradiation creep deformation with stress is predicted from the Preferred Absorption Glide (PAG) mechanism of irradiation creep [13]. In the case of the SIPA mechanism, the stress enters once in the interaction of the dislocation with an external stress; in the case of the PAG mechanism, the stress enters as in the SIPA mechanism and again in the glide of dislocations under the influence of the external stress. These parametric dependencies are shown in the following equations:

$$\dot{\epsilon}_{SIPA} = \frac{2}{9}\Omega D_i C_i \frac{\sigma}{E} L \Delta z_i^d \qquad (3)$$

$$\dot{\epsilon}_{CAG} = \frac{4}{9}\frac{\Omega}{b}(\pi L)^{1/2} D_i C_i \left(\frac{\sigma}{E}\right)^2 \Delta z_i^d \qquad (4)$$

where :

$\epsilon_{SIPA, CAG}$	=	creep strain rate for the SIPA and PAG mechanisms, respectively
Ω	=	atomic volume
b	=	Burgers vector
L	=	dislocation line length
D_i	=	interstitial diffusivity
C_i	=	interstitial concentration
σ	=	applied stress
E	=	elastic modulus
Δz_i^d	=	dislocation bias for interstitials

The quadratic dependence only becomes apparent at high stress levels and could explain the break away from linear dependence on stress that is observed. Thus, what appears to be bilinear curves in Figures 8 and 9 may actually be linear curves from SIPA creep on which parabolic curves from PAG creep are superimposed. The parabolic curve would dominate only at high stresses. The non-linear creep was not observed at the two lower temperatures, however. This might be expected since, at 400°C, the defect clusters of the lower temperature irradiation microstructure are replaced by glissile dislocations so that the effect of glide following climb becomes more dominant.

Summary

This experiment has demonstrated some previously unobserved phenomena associated with irradiation creep. Perhaps the most significant is the non-linear dependence of irradiation creep on stress at high stress levels in ferritic steels. This class of alloys was previously thought to be low in swelling and low in irradiation creep. No evidence suggests anything different with respect to swelling, but the data from the present study show that at 400°C HT9 has a higher rate of irradiation creep at stresses above 250 MPa than do the austenitic stainless steels. Although the data generated in this study are very limited, they are consistent with the observation of Troyanov et al. in another bcc metal, V-4Cr-4Ti [20]. Perhaps the enhancement of irradiation creep at high stresses is a general characteristic of bcc metals. This effect must be further investigated before ferritic steels can be used in a fusion reactor.

The minimum in irradiation creep deformation experienced in the laboratory heats of ternary alloys is a very interesting phenomenon. The stresses at which the minimum occurs are very low so that even though the effect may well be real, it is probably not significant in the application of this class of alloys to fusion reactors. It remains to explore this effect using electron microscopy to identify any precipitates that might be present in order to understand the effect.

The reduced level of irradiation creep at 200°C observed at the lower fluence level was confirmed at 19 dpa. Although the 60°C tubes did not yield data at 19 dpa that could be interpreted, the high creep rates observed at 7 dpa have not been contradicted. Further analysis of the 60°C tubes will be conducted to explore relationships at 19 dpa with the previous data at 7 dpa; however, too few tubes may remain pressurized to yield meaningful results. The behavior observed at 330 and 400°C in the austenitic stainless steels is consistent with previous results, and the presence of the fusion reactor level of helium makes this set of data the most relevant to the design of fusion devices available at the present time. Further research will focus on the low temperature regime to confirm the existence of high rates of irradiation creep in other alloys and at higher fluence levels.

ACKNOWLEDGMENTS

This research was sponsored by the Office of Fusion Energy Sciences, U.S. Department of Energy, under contract DE-AC05-96OR22464 with Lockheed Martin Energy Research Corporation. The authors also wish to express appreciation to W. S. Eatherly, G. W. Parks, and J. R. Gilley for assisting with the experimental work. The authors are also grateful to K. Farrell and J.P. Robertson for reviewing the manuscript and making many helpful suggestions.

REFERENCES

[1] Hesketh, R. V., Proceedings on Solid State Physics Research with Accelerators, Brookhaven National Laboratory, Upton, New York, 1967, p. 389.

[2] Konobeevsky, S. T., Pravdyuk, N. F., and Kutaitsev, V. I., Proceedings of Peaceful Uses of Atomic Energy, Vol. 7, United Nations, Geneva, 1955, p. 433.

[3] Grossbeck, M. L., Mansur, L. K., and Tanaka, M. P., Effects of Radiation on Materials: 14th International Symposium, ASTM STP 1046, Vol. II, American Society for Testing and Materials, Philadelphia, 1989, p. 537.

[4] Grossbeck, M. L., and Mansur, L. K., Journal of Nuclear Materials, Vol. 179-181, 1991, p. 130.

[5] Hamada, S., Maziasz, P. J., Tanaka, M. P., Suzuki, M., and Hishinuma, A., Journal of Nuclear Materials, Vol. 155-157, 1988, p. 838.

[6] Grossbeck, M.L. and Horak, J. A., Journal of Nuclear Materials 155-157 (1988) p. 1001.

[7] Tanaka, M. P., Hamada, S., Hishinuma, A., and Maziasz, P. J., Journal of Nuclear Materials, Vol. 155-157, 1988, p. 801.

[8] Lee, E. H., and Mansur, L. K., Philosophical Magazine, Vol. A 61, 1990, p. 751.

[9] Greenwood, L.R., Baldwin, C.A., and Oliver, B.M., Fusion Materials: Semiannual Progress Report for Period Ending September 30, 1994, USDOE, DOE/ER-0313/17 (1995) p. 28.

[10] Stoller, R. E., Grossbeck, M. L., and Mansur, L. K., Effects of Radiation on Materials: 15th International Symposium, ASTM STP 1125, American Society for Testing and Materials, Philadelphia, 1992, pp. 517-529.

[11] Gilbert, E. R. and Blackburn, L. D., Trans. ASME, Journal of Engineering Materials & Technology 99 Series H, No. 2(1977) p. 168.

[12] Mansur, L. K. Nuclear Technology, Vol. 40, 1978 p. 5.

[13] Mansur, L. K. Philosophical Magazine, Vol. A 39, 1979, p. 497.

[14] Bates, J. F. and Johnston, W. G., Radiation Effects in Breeder Reactor Structural Materials, AIME, New York, 1977, p. 625.

[15] Maziasz, P. J. in Phase Stability During Irradiation, AIME, New York, 1981, p. 477.

[16] Puigh, R. J. and Wire, G. L., Topical Conference on Ferritic Alloys for Use in Nuclear Energy Technologies, Snowbird, Utah, USA, AIME, New York, 1984, p. 601.

[17] Wassilew, C., Herschbach, K, Materna-Morris, E., and Ehrlich, K. Topical Conference on Ferritic Alloys for Use in Nuclear Energy Technologies, Snowbird, Utah, USA, AIME, New York, 1984, p. 607.

[18] Puigh, R. J., and Garner, F. A., Effects of Radiation on Materials: 14th International Symposium (Vol. II), STM STP 1046, ASTM, Philadelphia, 1990, p. 527.

[19] Kohyama, A., Kohno, Y., Asakura, K., Yoshino, M., Namba, C., and Eiholzer, C.R., Journal of Nuclear Materials 212-215 (1994) p. 751.

[20] Troyanov, V. M., Kruglov, A. S., Pevchykh, J. M., Bulkanov, M. G., Faskullin, V.A., Krjuchkov, E. A., Nikulin, M. P., Smirnoff, A. A., Rosanov, A. E., and Votinov, S. N., Proceedings of the Seventh International Conference on Fusion Reactor Materials, Obninsk, Russia, September 25-29, 1995, to be published by Journal of Nuclear Materials.

DISCLAIMER